EUROPEAN ORGANIZATION FOR NUCLEAR RESEARCH

CERN-EP/85-131

14 August 1985

INFLUENCE OF TRANSITION RADIATION AND DENSITY EFFECT ON ATOMIC K-SHELL EXCITATION

J.F. Bak, J.B.B. Petersen, E. Uggerhøj*), and K. Østergaard

Institute of Physics, University of Aarhus

DK-8000 Aarhus C, Denmark

S.P. Møller**) and A.H. Sørensen**)

CERN, CH-1211 Geneva 23, Switzerland

(Submitted to Physica Scripta)

---

*) Present address: CERN, CH-1211 Geneva 23, Switzerland.

**) Present address: Institute of Physics,
University of Aarhus,
DK-8000 Aarhus C, Denmark.

Abstract

A theoretical and experimental investigation is presented for the process of atomic K-shell excitation for GeV particles with special emphasis on the influence from the polarization of the surrounding target medium. During the last decade, a number of experiments have been performed to search for a 'density effect' in the vacancy production but all seem to have indicated its non-existence. This pattern was not broken until the recently published first data of the present series of measurements showed a pronounced but not the full effect on K-shell excitations in aluminum and copper targets. In the treatment given below the transition radiation emitted upon entrance into the target is shown to compensate partly the reduction due to the density effect. In this way inner-shell exciation yields are obtained which depend on penetrated depth into the target, e.g., with the net result that polarization effects may be neglected for thin samples. A simple relation is constructed which explains all existing experimental data. The large spread in γ values ($1 - 10^4$) for a GeV secondary beam has been exploited to measure the above relativistic effects in one single experiment. Here the simple model has proven to stand all tests including variation of target thickness, side of observation, and inclusion of a stack of foils to produce extra transition radiation upstream with respect to the target.

1. Introduction

When a charged particle traverses matter, it loses energy through collisions with target atoms. For swift particles, only electronical excitation and ionization processes need to be taken into account. In a classical impact-parameter description of such penetration phenomena, the collisions with target electrons are conveniently divided up into close and distant ones with a dividing impact parameter of the order of atomic dimensions. The energy lost by a particle passing through a target is the result of a large number of independent scattering events, so the process is a statistical phenomenon giving rise to an energy loss distribution which for thin targets consists of a Gaussian plus a high energy-loss tail. This tail is due to the close collisions where a large amount of energy is transferred to the target electrons. The most probable ionization energy loss, on the other hand, is determined alone by distant collisions. Besides an overall scaling with the square of the charge, this energy loss depends at relativistic energies only on the projectile, impinging with speed v, through the kinematical factors $\beta = v/c$ and $\gamma = (1 - \beta^2)^{-1/2}$.

The maximum impact parameter b_{max} for distant collisions increases proportional to γ and is large compared to atomic dimensions for $\gamma \gg 1$. Consequently, in dense targets there might be many atoms between the incident particle and the atom under consideration. These atoms are polarized in the presence of the projectile and the total electromagnetic field in the medium is reduced correspondingly. This so-called density effect results in a saturation of the most probable energy loss at high values of γ. The saturation - towards what is known as the Fermi plateau - was predicted already in 1940 by Fermi[1] and is by now well established theoretically and to a large extent also experimentally[2].

The above energy-loss phenomena are of course directly connected to the excitation and ionization cross-sections for the individual target electrons so

the strong influence of target polarization should also be found in measurements of the latter. This fact was first pointed out by Dangerfield[3], who based his theoretical investigations on a so-called Kolbenstvedt-type calculation[4]. Here the distant collisions are treated by the Williams-Weizsäcker method of virtual quanta[5-6], and Dangerfield could compute the influence of the target medium through the introduction of a dielectric function which modified the virtual photon spectrum. By adding the corresponding cross-section to that obtained for close collisions, a total ionization cross-section, which showed a saturation at high projectile energies, was obtained.

Experimental searches for the density effect in inner-shell excitations have been performed with electron impact[7-12] because in this case saturation effects are expected already at moderate MeV energies. However, the puzzling outcome of these previous investigations was that although reasonable agreement with theory was found elsewhere for the most probable energy loss, no density effect was seen in inner-shell excitations for electron energies up to as much as 2 GeV.

In order to cover a large range of γ-values (1 - 10^4), previous experiments were performed at different accelerators, whereby measurements of absolute cross-sections were needed. In the present series of experiments the large spread of γ-values is obtained in one single set-up because a 1 - 10 GeV/c secondary beam from a high-energy accelerator contains a mixture of protons, pions, and positrons, thereby covering γ-values ranging from around 1 to 10^5. For 1 - 10 GeV/c protons, density effects can be ignored so that the onset of such effects can be measured by measuring pion- and positron yields relative to those of protons. The relative measurements are, of course, depending on accurate particle identification which is possible in the present energy region. The first series of the present experiments on copper and aluminum targets were reported in a recent publication[13]. For the first time some density effect was

found for K-shell excitations, although not as much as expected from calculations with 'full' effect.

The apparent discrepancies encountered by all authors between theory and experiments lead to a reconsideration of the theoretical and experimental situation. Through this work, it was realized that the many speculations brought up by other authors to explain the lack of the density effect, should be discarded. Further on, it became clear that full density effect is not reached until after some depth in the target and that, during the setting up of the polarization fields, transition radiation (TR) is emitted, which acts as an x-ray source located in the surface region of the target. This recognition led to a new theoretical model in which inner-shell excitation caused by the emitted transition radiation as well as the gradual onset of the density effect was included and good agreement between measured and calculated yields was obtained[13].

In the present paper experimental results published for K-shell excitations caused by ultrarelativistic charged projectiles are reviewed. A short description of the new theoretical model is given, a detailed account will be published elsewhere[14]. The model is shown to explain all the previous data, including those reported in ref. 13, as well as to stand new experimental tests to be presented below. A description of the experimental procedure used in the latter and in our earlier investigations[13] is given in section 2. In section 3 follows a presentation of the experimental findings recorded by other authors and comments are given on some of the many ideas that have been put forward in order to explain the lack of the density effect. The short presentation of the theory of inner-shell excitation in the GeV region appears in section 4. The results of the new experimental tests are presented in section 5. Together with all previous data they are shown to confirm the new model. The tests contain measurements of K-shell excitation yields both on the incidence and the exit side of targets of varying thickness and the influence of transition radiation is investigated in a direct way by mounting a stack of two thin foils in front of the target.

2. Experimental Procedure

2.1 General layout

The experimental apparatus was installed in the t_7-beam of the CERN 28 GeV/c Proton Synchrotron. A schematic layout of the experiment can be seen in fig. 1. The beam was a high-intensity ($\sim 3.10^5/cm^2/sec$) secondary, non-separated, charged particle beam with a momentum adjustable between 1 and 10 GeV/c. Momentum slits allowed a reduction of intensity to limits acceptable for the detectors. In the positive polarity at 5 GeV/c, the beam consisted of approximately 30% protons, 60% pions, 8% positrons, and less than 2% kaons and muons. The beam divergence was $\sim\pm 0.5$ mrad and the size at the target was FWHM $\sim$ 20 mm.

Particle identification was performed in two ways: Two threshold Cherenkov counters were tuned for electron/muon and pion/kaon separation so that the $\sim$1% muons were included in the 60% pions and the $\sim$1% kaons in the 30% protons. In this way the errors introduced by the muon and kaon content of the beam was less than the statistical uncertainties. In the present experiment, particle identification is essential, so the positrons were also identified using a lead glass array at the end of the set-up.

Scintillation counters were used to define the usable fraction of the beam so as not to exceed the maximum size of the targets. The incoming particle trajectories were measured by a set of drift chambers. The incident beam line and target chamber were evacuated to better than 10^{-5} torr to reduce background and scattering. The targets were tilted 45° to the beam. In front and behind the target, two x-ray detectors were mounted at $\pm 20°$ to the surface normal, see fig. 1. Hereby maximum effective target thickness is obtained. To reduce the background, the targets were mounted on 80 x 120 mm^2 frames, which were much larger than the beam profile. The 10 mrad bend eliminated background from photons created upstream in scintillators, drift chambers, and mylar windows.

It may be noted that K-shell vacancies created by synchrotron radiation photons from this magnet can be neglected.

2.2 X-ray detectors, x-ray spectra, and background

In the present investigations, targets of copper and aluminum of thickenss 10 - 50 μm have been used. The x-rays were detected with conventional gas flow proportional counters (Siemens). The entrance windows were 2 μm mylar foils supported by a metal mesh with a transmission of 70%. For the copper K x-rays of ~8 keV, an argon/methane (90%, 10%) mixture was used, whereas pure propane was used to detect the aluminum K x-rays of ~1.5 keV. The high voltage on the counters was ~1.5 kV and ~2.8 kV for the case of copper and aluminum, respectively. Spectra from one of the front and one of the back detectors are shown in fig. 2. With a detector resolution of ~15% FWHM for the copper case and ~30% in the aluminum case the peaks contain both K_α and K_β x-rays. The argon escape peak is visible in the copper spectrum.

It is important to distinguish between two kinds of background: (i) the direct background of δ-rays, created in the target by the projectile, entering the x-ray detectors, and (ii) characteristic x-rays created by bremsstrahlung photons and δ-rays. The direct background, which is essentially projectile independent, gives rise to a continuous slowly varying spectrum, which can be eliminated when fitting the spectra (see below). The fact that the continuous background is reduced by an order of magnitude by removing the target, and that it is dominating behind the target means, that it is mainly due to δ-rays originating in the target itself. On the other hand, the background of characteristic x-rays can not be separated from the projectile-induced ones. We shall return to this problem in section 5.

Events giving a signal in one of the x-ray detectors within ~±0.5 μsec from the arrival of the projectile were recorded on magnetic tape, together with a

fraction of the total beam for normalization purposes. A narrow time-window (~150 ns and ~300 ns for the propane and the argon/methane mixture, respectively) was put around the prompt signals in the off-line analysis to get the final spectra of which fig. 2 is an example. The direct background is much lower in the aluminum than in the copper spectra since the use of the propane gas in the detector leads to better time resolution and lower efficiency for high energy photons. Also the lower atomic number and electron density reduces the background in the aluminum case.

The x-ray yields were extracted from the spectra for each detector in the following way. First a linear background plus a Gaussian was fitted to the total x-ray spectrum due to all three kinds of projectiles. Then this curve was fitted to the spectra belonging to each class of particles separately, keeping the position and the width of the Gaussian fixed together with the slope of the background (a fit is superimposed on the spectra on fig. 2). In this way the effect of the statistical uncertainties on the background determination was minimized. By making reasonable variations in the background, the uncertainty in its subtraction was estimated to be a few percent, and thus less than the statistical ones.

3. Previous Results and Proposals to Explain the Lack-of-the-Density-Effect Mystery

In fig. 3 are shown the results from earlier experiments on copper and aluminum targets together with theoretical estimates as obtained in what is generally known as a Kolbenstvedt-type approach, cf section 4.1 to follow. The full drawn curves show the calculated cross-sections as a function of γ for the cases when 'full' density effect is expected. The dashed curves show the cross-sections, when density effect is disregarded. From the curves it is clear that density effect should set in for electrons already at a few MeV for incidence on

aluminum targets and at around 100 MeV for impact on copper targets. The earlier experiments clearly show no evidence of the effect for electron energies up to as much as 2 GeV, a result which also holds for all other target materials investigated. In order to explain this mystery, various more and less plausible ideas have been brought up through the last years.

Since the density effect appears as a result of target polarization, described through the introduction of a frequency dependent dielectric function $\varepsilon(\omega)$, the various proposals for its non-appearance have all been based on modifications of this response function. The deviation of ε from its vacuum value 1 determines the strength of the polarization so that a smaller value of $1 - \varepsilon(\omega)$ corresponds to smaller density effect. Only photons with energies exceeding $\hbar\omega_K$, the minimum excitation energy of the K-shell electron, may contribute to the yields in question. For $\omega > \omega_K >> \omega_p$, a simple expression for $\varepsilon(\omega)$ may be obtained, namely

$$\varepsilon(\omega) = 1 - \omega_p^2/\omega^2 \ , \qquad \omega_p^2 = 4\pi ne^2/m \ , \tag{1}$$

where ω_p denotes the plasma frequency of the target electron gas of density n and m the electron rest mass (cf section 4.2). Since the density effect is expected to set in for γ values around ω_K/ω_p, as we shall discuss in section 4, the lack of density effect for electrons with an energy as high as 2 GeV would require a reduction of ω_p by a factor of 10 or more. Such a reduction was was proposed by Tawara[15] who argued that only the two K electrons could screen for $\omega > \omega_K$. In this way an effective plasma frequency of $(\omega_p^{eff})^2 = 2\omega_p^2/Z$ was introduced for a given medium of atomic charge Ze. The assumption of Tawara, however, is rather questionable since for $\omega > \omega_K$ all electrons effectively are free and take part in the screening - especially the very loosely bound outer

shell ones. Indeed, the expression (1) is the one encountered for a free electron gas.

Kamiya et al.[12] defined another effective plasma frequency for virtual photons, namely $(\omega_p^{eff})^2 \propto \omega_p^2(\lambda/a)^3$ where λ denotes the wavelength of the virtual photon and a is the lattice constant of the medium. Here, the idea is that the expression (1) for the dielectric function valid for real photons might not hold for virtual ones with wavelengths comparable to or smaller than a. The point to discern between real and virtual photons when calculating the response of a solid is somewhat dubious, however, because ε simply describes the reaction of the medium to a given electric field.

Amundsen[16] suggested that the deep core electrons, being strongly localized, cannot screen at frequencies corresponding to $\lambda \lesssim a$. This gives a cut-off in ε for frequencies exceeding the value $\omega_a = \pi c/a$. Since ω_a typically attains values of 1 - 1.5 keV, this means that no density effect is expected for K-shell excitation in elements heavier than, approximately aluminum.

How would such modifications of the dielectric function compare with direct measurements? Above the K-shell threshold it is in general difficult to extract reliable information on $1 - \varepsilon$ from measurements of the index of refraction $n = \sqrt{\varepsilon}$ since $1-n \simeq (1 - \varepsilon)/2 = (\omega_p/\omega)^2/2 < (\omega_p/\omega_K)^2 \lesssim 10^{-3}$. Sufficiently accurate measurements of n do not seem to be available and the validity of the above proposals needs to be checked in another way.

Much better information about a possible cut-off in $\varepsilon(\omega)$ is obtained from physical phenomena which depend directly on $1 - \varepsilon$. For this purpose, transition radiation offers an excellent tool because this well-known radiation is emitted when a charged particle traverses the interface between two dielectrics and therefore is just caused by the difference in $\varepsilon(\omega)$ values in the two media, which could be vacuum/solid target. In connection with particle identification studies for GeV particles, transition radiation has been studied in great detail and is discussed in several papers. Here, we consider the measurements by Cobb et al.[17], where 1.34 GeV/c electrons traverse an array of 499 Li foils.

In this reference measured and calculated spectra are shown, from which it is clear that the radiation goes far beyond the cut-off of 1 - 2 keV, predicted by Amundsen, and therefore contradicts his idea. It also contradicts the ideas of an effective plasma frequency $\omega_p^{eff} \sim \omega_p/10$ because the transition radiation spectrum in this case would extend only up to $\sim \gamma\hbar\omega_p^{eff} \sim 4$ keV rather than to the experimentally confirmed value of $\sim\gamma\hbar\omega_p \sim 37$ keV.

In ref. 13 we further discussed how our own measurements of the constancy of the Fermi plateau encountered for the most probable energy loss in silicon and germanium excluded lack of density effect for K- and other inner-shell electrons. In fact, much older empirical data exists, which relate closely the ionization energy loss to the process of inner-shell excitation. Figure 4 shows the ionization energy loss of relativistic muons and electrons in helium recorded in a cloud chamber by Kepler and co-workers in 1957 (ref. 18). Evidently, loss of energy here proceeds via excitation of K electrons. In the experiment the maximum energy transfer amounted to a fixed value of 0.74 keV whereby the γ-dependence of the loss rate only survived in the distant encounter contribution. Correspondingly, the data of fig. 4 increases with increasing energy proportional to log γ in the region $\gamma \gtrsim 10$, until saturation towards the Fermi plateau sets in at $\gamma \sim 10^2$.

4. Theory

The density effect is expected when the electromagnetic field of a relativistic, charged projectile is substantially different in vacuum and (deep) inside the considered target. Exactly in this situation, however, transition radiation is emitted in the process of adjusting the fields at the target surface[6]. As pointed out in our previous publication[13], the appearance of TR tends to some extent to compensate the density effect. Correspondingly, for K-shell excitation it was discussed how the lack of the effect observed by other authors

as well as the pronounced but not full effect reported in ref. 13 could be understood when account was taken of excitation caused by the created TR.

In this section, we shall derive the simple, approximate relation quoted in our previous paper[13].

4.1 General framework

In the calculation of inner-shell excitation yields we shall adapt a procedure introduced by E.J. Williams[5]. In his treatment, Williams divides collisions between the projectile and the atom under consideration into two groups, so-called close and distant ones. Correspondingly, the cross-section is split into two parts,

$$\sigma = \sigma_c + \sigma_d \ . \tag{2}$$

The contribution σ_d from distant collisions is determined by application of the Williams-Weizsäcker method of virtual quanta[5,6]. As a result, the dividing distance, d, between close and distant encounters, the length of which is of the order of atomic dimensions, appears in the argument of a usually large logarithm and the exact choice is not important. Following Williams we choose $d = (\hbar/2m\omega_K)^{1/2}$, which quantity essentially reflects the radius of the electronic orbit under consideration. For the close collisions, where the perturbative treatment breaks down, the momentum transfer to the target electron attains values $\gtrsim \hbar/d$ which leads to an energy transfer in excess of the minimum excitation energy, $w \gtrsim \hbar\omega_K$, with the above choice for d. Hence the contribution σ_c essentially may be obtained from the differential cross-section $d\sigma_f/dw$ for collisions between free particles as

$$\sigma_c = \int_{\hbar\omega_K}^{w_{max}} dw \frac{d\sigma_f(w)}{dw}, \tag{3}$$

where the maximum energy transfer w_{max} is determined by the kinematics. Clearly, σ_c is independent of target polarization.

The basic idea of the virtual photon method is to replace the perturbing fields of a rapidly moving projectile by an equivalent pulse of radiation and then calculate the interaction between this projectile and the target through known cross-sections for photon interactions[5,6]. For our case, the relevant cross-section is σ_γ^K, the photoelectric cross-section for K-shell excitation and, correspondingly, σ_d is given as

$$\sigma_d = \int_{\omega_K}^{\infty} d\omega \cdot \frac{1}{\hbar\omega} \frac{dI}{d\omega} \sigma_\gamma^K(\omega) \quad . \tag{4}$$

Here the intensity $dI/d\omega$ of virtual photons of frequency ω reflects the polarization of the medium since it is defined by the Fourier component of the total electromagnetic $\vec{E}$-field as

$$\frac{dI}{d\omega} = c \int_d^{\infty} d\varrho \cdot \varrho \cdot |\vec{E}(\omega)|^2 \tag{5}$$

where ϱ denotes the impact parameter of the projectile relative to the atom.

In the literature on inner-shell excitation the application of the above scheme, eq. (2), where the distant collision contribution is determined by means of the virtual photon method is often denoted the "Kolbenstvedt method" although the difference between the treatment given by this author[4] and the original work of Williams lies only in the choice of the specific expressions for the cross-sections $d\sigma_f/dw$ and σ_γ^K. With a proper choice of the latter[14] the accuracy of the method at the high γ-values of interest in the present context is comparable to that of much more elaborate theories, cf. ref. 14.

4.2 The simple relation quoted in ref. 13

In order to discuss the influence of the polarization of the target medium on the process of K-shell excitation an explicit expression for the dielectric function $\varepsilon(\omega)$ is needed. Since we are interested only in frequencies above the K-edge, $\omega > \omega_K$, that is, in frequencies above all atomic resonances, the screening electrons respond essentially as a free electron gas. Correspondingly, the result (1) is assumed to apply.

For a projectile of unit charge moving in an infinite medium characterized by the simple dielectric function, eq. (1), the virtual photon spectrum reads[3,14]

$$\frac{dI^{M\infty}}{d\omega} = \frac{2}{\pi}\alpha\hbar\beta^{-2}\left\{\log\left(\frac{1.123c}{d\cdot\omega}\left[(\beta\gamma)^{-2} + \frac{\omega_p^2}{\omega^2}\right]^{-1/2}\right) - 1/2\right\} \tag{6}$$

for frequencies large compared to the plasma frequency, $\omega \gtrsim \omega_K \gg \omega_p$. For the special case of motion in vacuum, eq. (6) reduces to

$$\frac{dI^{V}}{d\omega} = \frac{2}{\pi}\alpha\hbar\beta^{-2}\left[\log\left(\frac{1.123c\cdot\beta\cdot\gamma}{d\cdot\omega}\right) - 1/2\right]. \tag{6'}$$

For γ's lower than the critical value

$$\gamma_c \equiv \omega/\omega_p \tag{7}$$

the virtual photon spectrum, eq. (6), is essentially unaffected by medium polarization and given by the vacuum value, eq. (6'), which increases with log γ. On the other hand, for $\gamma > \gamma_c$, the spectrum $dI^{M\infty}/d\omega$ saturates into a γ-independent constant. This reduction is known as the density effect, the

limiting value of the spectrum being intimately connected to the so-called Fermi-plateau reached at high values of γ in the most probable ionization energy loss. For the considered targets γ_c attains values of

$$\gamma_c \gtrsim \gamma_c^K \equiv \omega_K/\omega_p = \begin{cases} 47 & , \text{Al} \\ 154 & , \text{Cu} \end{cases} \tag{7'}$$

So far, we have only considered the projectile as moving in an infinite medium. The density effect appears as a result of a shortening of the range of the electromagnetic fields inside the target medium with respect to that encountered outside in vacuum. Consequently, a significant adjustment of the fields must take place near the target surface. In this process transition radiation is emitted[6,19]. Since the TR is emitted in the very near forward direction, all radiation created at the incidence surface enters the target whereas that created at the exit side, for high values of γ outside in vacuum, never reaches the target medium. In the following we shall therefore consider only TR created at the incidence side.

The TR spectrum for a vacuum-medium interface is given, e.g., by Jackson[6] as

$$\frac{dI^{TR}}{d\omega} = \frac{2}{\pi}\alpha\hbar\left\{\left[1/2 + \left(\frac{\omega}{\gamma\omega_p}\right)^2\right]\log\left[1 + \left(\frac{\gamma\omega_p}{\omega}\right)^2\right] - 1\right\}, \tag{8}$$

the expression being valid for $1 - \beta \ll 1$. For $\gamma < \gamma_c$ where no density effect appears, i.e., where $dI^{M\infty} \simeq dI^V$, the TR spectrum falls off very rapidly since essentially no field adjustment takes place.

As the target electrons get excited by the real TR photons as well as the virtual ones, we should in the calculation of the yields according to eq. (4) rather use the total photon spectrum than simply $dI^{M\infty}/d\omega$. Since the real TR

photons get absorbed, their characteristic absorption length being $\lambda_a(\omega)$, the total photon spectrum to enter eq. (4) is given by

$$\frac{dI^{tot}}{d\omega} = \frac{dI^{M\infty}}{d\omega} + \frac{dI^{TR}}{d\omega} \exp\left[-z/\lambda_a(\omega)\right] , \tag{9}$$

where z denotes the distance along the projectile path travelled beyond the target surface. Using the expressions (6), (6'), and (8), it immediately follows that

$$\frac{dI^{M\infty}}{d\omega} + \frac{dI^{TR}}{d\omega} = \frac{dI^{V}}{d\omega} - C ,$$

$$C \simeq \frac{2}{\pi} \alpha\hbar \begin{cases} 1 \text{ for } \gamma > \gamma_c \\ 0 \text{ for } \gamma < \gamma_c . \end{cases} \tag{10}$$

Since the quantity in square brackets in (6') typically attains values of order 10, the correction term C in (10) may often be neglected.

The simple result for the onset of the density effect, as expressed through the equations (9-10), may be questioned in view of the naive derivation given here. However, as demonstrated in ref. 14 where a thorough theoretical investigation is presented, the dependence of the inner-shell excitation yield on penetrated depth is well described through application of the relations (9-10).

5. Experimental Results

According to the above discussion it is now clear that for targets thin compared with the absorption length $\lambda_a(\omega)$ no density effect may be observed since $dI^{tot} \simeq dI^{V}$. This explains the experimental results reported by other authors, fig. 3, where such targets were used. Because of common systematic errors, however, the relative increase of yield with primary energy reported in

ref. 11 for 0.9-2.0 GeV electrons is determined with higher accuracy than the absolute cross-sections, making the trend at high γ significant. With full density effect we should expect no increase since $\gamma \gg \gamma_c$. Neglecting the density effect the increase should, on the other hand, amount to $\sim$ 8%. The experiment in ref. 11 was performed in a total of three runs under different experimental conditions. For the last one, the recorded increase was 5-11% for the variety of target materials investigated. Hence the value corresponding to absence of the density effect is recovered. However, for the first two runs the increase observed was, with only one exception, 3-4 times as strong. We shall return to this feature in section 5.2.

In our previous work[13] we measured the K-shell excitation yield for 5 GeV/c proton, pion, and positron impact on copper and aluminum targets, thick compared with λ_a, in a geometry similar to that presently used with a single detector placed at the front side of the target. The results, all normalized to that encountered for protons, are repeated in fig. 5 (open circles). In order to compare with theoretical predictions, as well as with the previous measurements presented in fig. 3, we have normalized both of the latter to a theoretical cross-section computed for 5 GeV/c protons. Here we used values provided by Amundsen and Aashamar[20] since the virtual photon scheme gives less accurate answers for $\gamma \lesssim 10$ (cf. also ref. 14). As is clear from fig. 5, our findings demonstrated, for the first time, the presence of some, but not the full, density effect.

The target thickness used in ref. 13, the absorption length of K_α x-rays, as well as the absorption length on top of the K-edge are given in table 1 for each of the two considered targets. Taking into account the actual target geometry and the self absorption of the triggering K x-rays, where the slight difference for the K_α and the minor K_β component is immaterial, the dot-dashed curves of fig. 5 were produced on the basis of the simple model described in section 4 and corresponding to the photon intensity given in eq. (9). The

agreement between our experimental results and this simplified theory is fair, and especially convincing for the heavier target material.

5.1 Dependence on target thickness and site of observation

After this success, a second series of experiments were designed in order to explore further the validity of our theoretical model. As a first test we tried to determine the variations in K-shell excitation yield with target thickness and to measure the differences encountered by detectors placed at the incidence and the exit side of the target. Clearly, with increasing target thickness the findings are expected to approach the full density effect curve since the fraction of the target, where no density effect occurs, decreases. Further, due to the self-absorption of the outgoing x-rays, the side of the target facing the detector has the higher weight and hence we expect to observe a larger yield for positrons at the incidence than at the exit side. In the first two lines of table 2 we present our experimental results for the ratio of the positron to the proton yield at 5 GeV/c for an aluminum and two different copper foils together with theoretical predictions, where for the protons we again use the cross-section of Amundsen and Aashamar[20]. From the table it is clear that all the experimental results follow nicely the theoretical predictions. Note especially that the results for aluminum are significantly closer to our expectations than was the case in ref. 13.

The experimental uncertainties quoted in table 2 reflect the purely statistical ones. Also some errors might be introduced by background subtraction. From the x-ray spectra, however, it is clear that such errors are important only for the exit side detectors and, even here they seem not to exceed the statistical ones, cf., section 2. At this stage it should be noted that although the tendencies in the experimental results, reported in table 2, for given target material seem to agree essentially with our expectations, the

variations encountered might not be significant in view of the error bars which nearly overlap, e.g., in all the copper results. The problem appears since both copper foils have nearly the same effective thickness, $\sim \lambda_a(K_\alpha)$. In order to provide significant changes in the K-shell excitation yield, one target should instead be chosen thin compared with $\lambda_a(K_\alpha)$ but, unfortunately, with such a thin foil the total data taking period would be unacceptably long with the present set-up and at the same time severe background problems might be expected, cf., section 2.

It is worth stressing that the differences between the results measured for the two copper foils, table 2, for both surfaces are so small that effects depending on the square of the target thickness as, e.g., K-shell excitation caused by secondary δ-electrons or bremsstrahlung emitted by the primary positron, appear to be small enough to be hidden by the purely statistical errors. In an estimate of the direct bremsstrahlung contribution it suffices to compare the total intensity reaching a given point inside the target with the virtual photon intensity, eq. (6). In this way we get as upper bounds corrections of 0.2% and 4% for aluminum and copper, respectively, which are seen not to exceed the statistical errors. It should be noted that the direct bremsstrahlung tends to increase our positron K-shell excitation yields whereas the δ-electrons tend to decrease relative yields since their contribution is essentially particle independent and applies for proton impact, as well.

Using the latter observation, the importance of the δ-electron contribution, which is estimated to be smaller than, typically, 5%, may be investigated experimentally by considering the K-shell excitation yields for pions since for these the density effect, transition radiation, and bremsstrahlung will not be present. The results are shown in the lower half of table 2. Essentially, no difference is encountered neither for the incidence nor for the exit side between the yields measured for the two different copper foils. Although for a

given target the differences between incident and exit side detectors show the right sign, at least in the measurements on copper, the statistical error bars are still overlapping (notice also that the thicker target shows the minor variation). The overall conclusion of our analysis of the experimental results presented in table 2 is then that the uncertainties on our experimental points are dominated by statistical fluctuations.

5.2 Inclusion of a stack of TR foils

In order to provide a more powerful and sensitive check of the theoretical model for the interplay between the density effect and created TR, a second experiment was set up. Here a stack consisting of two thin copper foils was placed at right angles to the beam upstream with respect to an ordinary 25 μm copper target for which the yield of K x-rays was measured both at the incidence and the exit side. In such an arrangement the yields should increase with an amount corresponding to the difference between the dot-dashed and the full drawn curves of fig. 5 times the enhancement for frequencies around ω_K of the TR created in the stack over that created at a single surface (the target incidence surface). For a single copper foil, when absorption is neglected, the maximal TR intensity emitted with $\omega \sim \omega_K$ is $\sim$ 94% of the yield corresponding to two single surfaces and it is reached for a thickness of 3.26 μm, cf., ref. 21. By choosing the spacing between the foils in the stack to be larger than $2\pi\ell_2$, where ℓ_2 denotes the formation length for a medium-vacuum interface, the TR created in the various foils may be added incoherently[21]. In our case the requirement was that the spacing should be larger than 3 cm. Taking into account absorption, the effective number of copper foils is very low. We therefore chose to work with a stack of only two, each having a thickness of 3 μm, their interspacing being 5 cm and the distance from the last foil to the tilted target being 9 cm. With this arrangement the expected enhancement over,

e.g., a curve corresponding to the dot-dashed of fig. 5 is roughly twice the difference between this and the full density effect plateau.

The experimental findings are presented in fig. 6. Together with the usual curves for full and no density effect, we further show our theoretical predictions, based on the simple model, for the relative K-shell excitation yield as it should be observed both on incidence and the exit side of the 25 μm copper target when the stack is introduced. In view of the large interspacings we have made the following replacement in eq. (9),

$$\frac{dI^{TR}}{d\omega} \rightarrow \frac{dI^{TR}}{d\omega} + \left(\frac{dI}{d\omega}\right)_{stack} . \tag{11}$$

Generalizing the formulaes given in ref. 21 to the case of strong absorption, i.e., to the case where the absorption length $\lambda_a(\omega)$ becomes comparable to the thickness t_f of a foil in the stack, the total TR intensity emerging from the stack takes the form

$$\left(\frac{dI}{d\omega}\right)_{stack} = \left(1 + e^{-t_f/\lambda_a(\omega)}\right) \times \left[\left(1 - e^{-t_f/2\lambda_a(\omega)}\right)^2 \frac{dI^{TR}}{d\omega} + e^{-t_f/2\lambda_a(\omega)} \frac{2}{\pi} \hbar\alpha G\right] \tag{12}$$

where the function G introduced in ref. 21 may be expressed analytically as

$$G = \frac{\pi}{\hbar\alpha} \frac{dI^{TR}}{d\omega} + \left[1+2\left(\frac{\omega}{\gamma\omega_p}\right)^2\right][\cos V\,ci(a) - \sin V\,si(a) - ci(a+V)] + 2\cos(a+V) + a[\cos V\,si(a)+\sin V\,ci(a)] + (a+V)si(a+V) , \tag{13}$$

$$a = \frac{t_f\omega}{2\gamma^2 c} , \qquad V = \left(\frac{\gamma\omega_p}{\omega}\right)^2 a$$

by introduction of the sine and cosine integrals si, ci (cf., refs. 22-23).

The experimental data presented in fig. 6 follow very closely the theoretical curves. Only the yield recorded at the exit side for positron impact is somewhat off, and this may be due to background problems. As to the yield recorded for the pions it may be noted that the deviations from the data presented in table 2 are within the statistical error.

A quite similar test of the influence of transition radiation on K-shell excitation yields seems to have existed in the experiment of Genz et al.[11]. Here data were produced for electron impact during two different sets of runs. In the last, the beam-line upstream and the target chamber were directly connected whereas in the first, each of these elements was closed-off with a kapton foil of thickness 50 μm and 100 μm, respectively, and separated by 7 cm of air. As correctly stated by the authors of ref. 11, the presence of the two extra foils and the air gap in the first runs leads to production of photons which, along with the projectile itself, may lead to K-shell vacancy production in the target. In order to correct for this, first a single stack of kapton foils and in turn an additional one was introduced into the air gap. Each stack had a thickness of $1.0 \cdot 10^{-3}$ radiation lengths corresponding to that of the two original foils and the air gap. With a total of three different measured x-ray yields an extrapolation to the case of no material in the beam line determined the correction. For nickel this was 13% at an electron energy of 900 MeV.

The authors indicate that the value of 13% is in agreement with estimates of the K-shell vacancy production due to bremsstrahlung photons emitted in the kapton foils and the air gap. To determine this correction it suffices within our model to compare the bremsstrahlung to the virtual photon intensity, in this case for vacuum since the target itself is very thin, and we do not need to worry about photo-cross-sections. In the soft photon region of interest, the bremsstrahlung intensity per incident electron, after the penetration of a material whose thickness is T radiation lengths, amounts to $\simeq 4/3\hbar T$. Relative

to the virtual intensity $dI^V/d\omega$ the correction is $\simeq 2\pi T/3\alpha L^V$, where L^V corresponds to the term in brackets in eq. (6'). For $T = 1.0.10^{-3}$ and with $L^V \gtrsim 10$ we arrive at a correction of $\lesssim 3\%$.

Apparently, bremsstrahlung does not account for the 13% correction in the first runs of the experiment by Genz et al. What could have magnified the γ-dependence - and given rise to the extra 10% background in the first runs? In view of the discussion which lead to the curves presented in fig. 6, it is clear that TR is a candidate. In kapton the absorption length just above ω_K for copper amounts to $\simeq 0.2$ cm which means that, in a first approximation, absorption may be neglected. Next, the foils are very thick compared with the formation length for TR as is their interspacing. This means that the total TR-intensity approximately equals the incoherent sum of the intensities created at each single surface[21]. Finally, since all γ values in the experiment of ref. 11 are below γ_c for air we may in our estimates substitute the air by vacuum gaps, which means that eq. (8) applies.

In the initial situation 4 TR-producing surfaces are present. Depending on the exact geometrical arrangement when introducing the additional stacks of kapton foils the extrapolation to zero foil material in the beam line corresponds to a correction for only zero to two surfaces while still four to two remain. At 900 MeV a correction for two surfaces amounts for copper to $\simeq$ 11% extra K-shell excitation yield, i.e., the effect is of the right size to explain the missing background contribution. Further, with two surfaces remaining the increase of the yield at 2 GeV over that encountered at 900 MeV would amount to 20%, which number again is compatible with the experimental findings.

The above discussion serves to stress the importance of careful examination of possible TR-sources which might be present in an experimental set-up. For the specific case we may mention that in our analysis we are faced with the problem that the correction applied in runs I, II depends linearly on the number

of stacks introduced, as demonstrated in fig. 8 of ref. 11, whereas the two immersed into the air gap at a distance of 0.3-0.4 cm from the foil sealing the target chamber have been mounted on top of each other[24], so as to introduce no extra TR-surfaces in going from one to two stacks.

6. Concluding Remarks

In conclusion we see that the simple theoretical model is compatible with practically all experimental tests performed so far no matter how large variations in K-shell excitation yields these show. The model thereby resolves the so-called lack-of-the-density-effect mystery which has persisted for a decade. The latest experimental tests serve as important proofs of the validity of the model.

A detailed experimental investigation still remains of the variation of the inner-shell excitation yield as the target thickness is gradually increased from the very thin foils used by other authors to the very thick ones used in the present investigations. Due to the low data-taking rate and background problems in a secondary beam such a program has not yet been initiated at CERN. This important experiment should be performed in a clean, well focussed high-energy electron beam. Further, the question needs an answer why the absolute measurements for copper reported in ref. 7 are higher than all theoretical predictions. Also the question is unanswered why our own results for aluminum for positron impact remain somewhat too high.

Acknowledgements

The authors wish to acknowledge the stimulation received through discussions with P.A. Amundsen, J.U. Andersen, and E. Lægsgård. We are also indebted to P.G. Hansen for his constant encouragement. The Danish participation in the collaboration was possible through support from the Danish Committee for Accelerator Physics.

References

1: E. Fermi, Phys. Rev. 57 (1940) 485.

2: A. Crispin and G.N. Fowler, Rev. Mod. Phys. 42 (1970) 290;
See also H. Esbensen et al., Phys. Rev. B 18 (1978) 1039 and ref. 6.

3: G.R. Dangerfield, Phys. Lett. A 46 (1973) 19.

4: H. Kolbenstvedt, J. Appl. Phys. 38 (1967) 4785.

5: E.J. Williams, Kgl. Danske Videnskab. Selskab, Mat.-Fys. Medd. XIII, No. 4 (1935).

6: J.D. Jackson, Classical Electrodynamics (Wiley, New York, 1975).

7: L.M. Middleman, R.L. Ford and R. Hofstadter, Phys. Rev. A 2 (1970) 1429.

8: G.R. Dangerfield and B.M. Spicer, J. Phys. B 8 (1975) 1744.

9: K. Ishii et al., Phys. Rev. A 15 (1977) 906.

10: D.H.H. Hoffmann et al., Z. Physik A 293 (1979) 187.

11: H. Genz et al., Z. Physik A 305 (1982) 9.

12: M. Kamiya et al., Phys. Rev. A 22 (1980) 413.

13: J.F. Bak et al., Phys. Rev. Lett. 51 (1983) 1163.

14: A.H. Sørensen, to be published.

15: H. Tawara, in: Proc. 10th ICPEAC, Paris 1977, ed. G. Watel (North Holland, Amsterdam, 1978).

16: P.A. Amundsen, Phys. Lett. A 89 (1982) 417.

17: J.Cobb et al., Nucl. Instrum. Methods 140 (1977) 413.

18: R.G. Kepler et al., Nuovo Cimento 7 (1958) 71.

19: G.M. Garibian, Sov. Phys. JETP 6 (1958) 1079.

20: P.A. Amundsen and K. Aashamar, J. Phys. B 14 (1981) L153 and private communication.

21: X. Artru, G.B. Yodh and G. Mennessier, Phys. Rev. D 12 (1975) 1289.

22: I.S. Gradshteyn and I.M. Ryzhik, Table of Integrals, Series, and Products (Academic Press, New York, 1965).

23: M. Abramowitz and I.A. Stegun, Handbook of Mathematical Functions (Dover, New York, 1972).

24: H. Genz, private communication.

Table 1

Thickness of the aluminum and copper targets used in ref. 13 together with the K_α-absorption length and the absorption length at the top of the K-edge. All lengths are given in μm.

Target	t	$\lambda_a(K_\alpha)$	$\lambda_a(\omega \to \omega_K+)$
Al	10	9.19	0.83
Cu	25	22.3	3.75

Table 2

Experimental and theoretical results for the K-shell excitation yield for 5 GeV/c positrons and pions relative to that for 5 GeV/c proton impact for three different targets.

Particle	Al 25 μm		Cu 25 μm		Cu 50 μm	
	front	back	front	back	front	back
e^+(exp)	1.87±.07	1.58±.09	2.22±.08	1.86±.09	2.11±.06	1.87±.08
e^+(th)	1.71	1.59	2.10	2.01	2.05	1.93
π^+(exp)	1.30±.03	1.39±.05	1.36±.04	1.28±.05	1.36±.03	1.31±.04
π^+(th)	1.41	1.41	1.47	1.47	1.47	1.47

Figure Captions

Fig. 1 Schematic drawing of the experimental set-up. The beam enters from the left. SC designates scintillators; DC, drift chambers; C, Cherenkov detectors; and LG, lead-glass array.

Fig. 2 A copper spectrum (a,b) and an aluminum spectrum (c,d) from one of the front (a,c) and one of the back (b,d) detectors. The fit, based on the dotted data points, used to extract the x-ray yields, is superimposed on the data.

Fig. 3 K-shell excitation yield as a function of γ for projectiles of unit charge impinging on solid targets of aluminum and copper. The full-drawn curves are calculated by inclusion of the dielectric response, eq. (1), whereas the dashed curves correspond to neglect of density effects. The experimental points are taken from refs. 7, 10-12. Note that the large error bars on the points of Genz et al.[11] are due mainly to uncertainties in the fluorescence yield and target thickness and hence the relative positions of these points are much better known than the error bars indicate.

Fig. 4 Ionization energy loss of electrons and muons in helium. Standard deviations are indicated for a few of the experimental points. Adapted from ref. 18.

Fig. 5 Same as fig. 3 but including the results reported in ref. 13. The dot-dashed curves correspond to the theoretical yields obtained on the basis of the simple model, eq. (9), for a foil thickness of 10 and 25 μm for the case of aluminum and copper, respectively.

Fig. 6 Normalized K-shell excitation yield for impact on a tilted 25 μ copper target when an open stack consisting of two 3 μm copper foils are placed upstream. The dot-dashed curves represent the theoretical results corresponding to observation at the incidence (upper curve) and exit side (lower curve) of the target. The corresponding experimental yields recorded for 5 GeV/c proton, pion, and positron impact are identified. The solid and dashed curves correspond to those given in figs. 3 and 5.

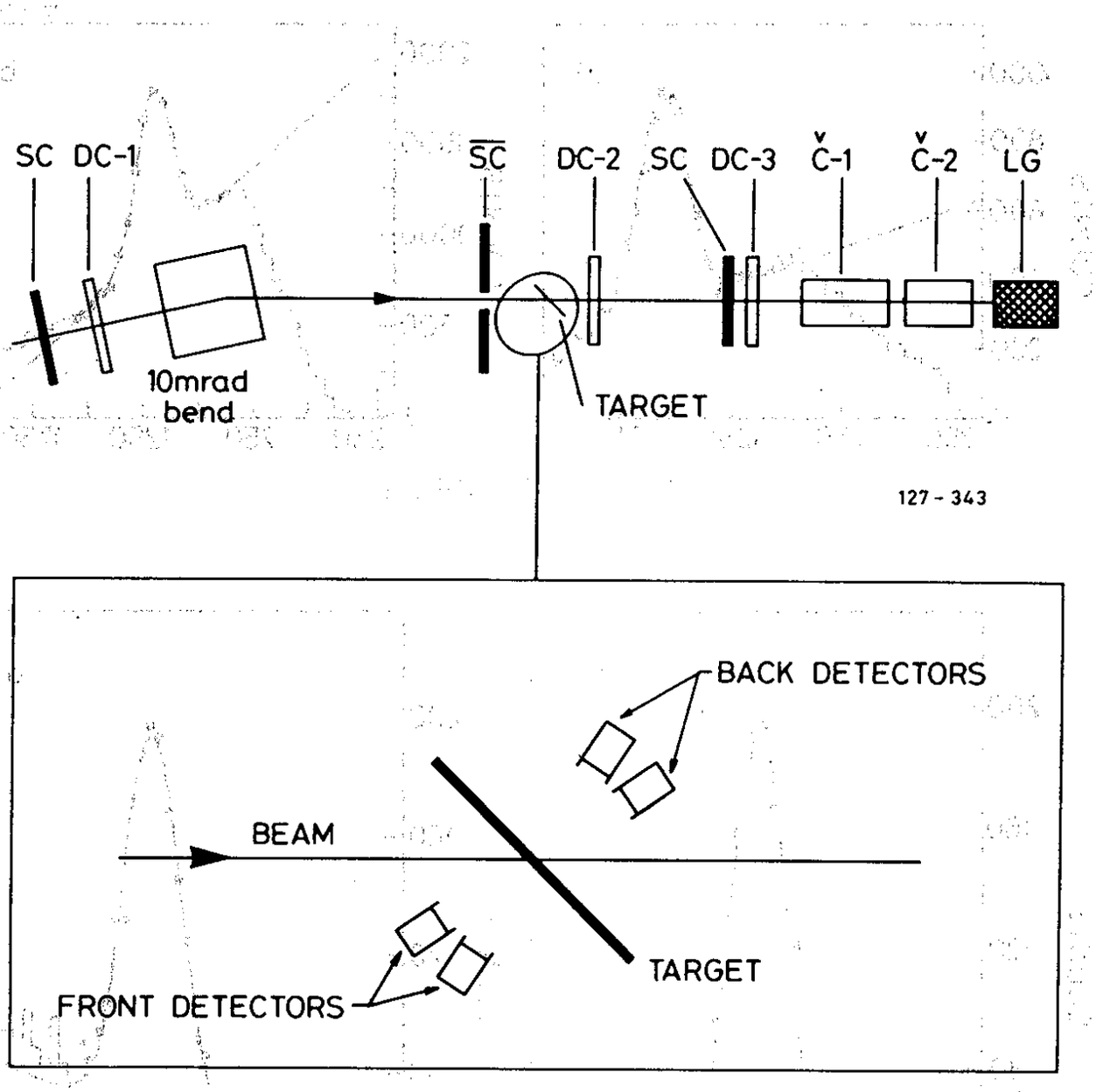
SC
DC-1
10mrad
bend
SC
DC-2
SC
DC-3
C-1
C-2
LG
TARGET
127 - 343
BACK DETECTORS
BEAM
TARGET
FRONT DETECTORS

Fig. 1

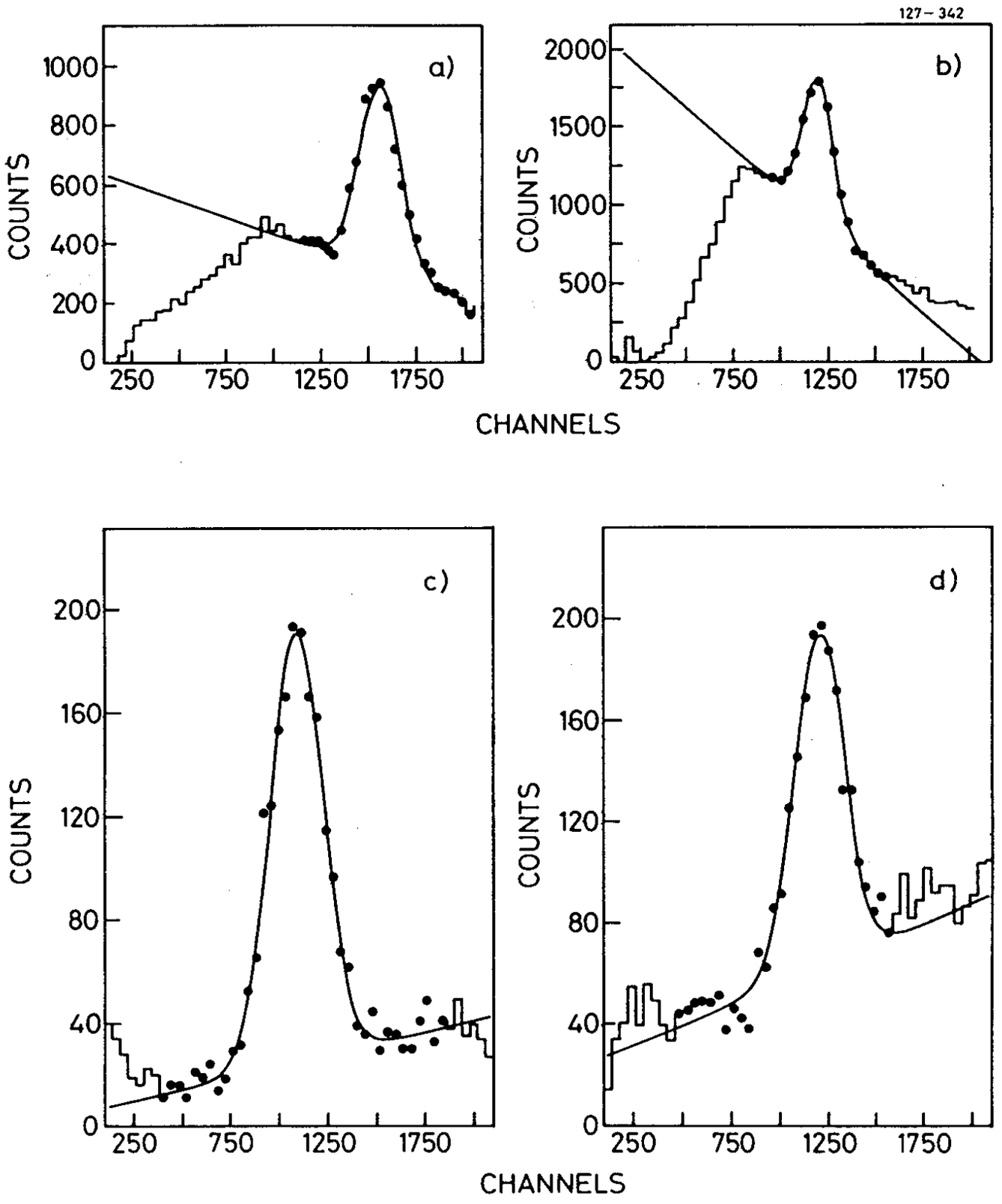
127-342
a)
b)
c)
d)
COUNTS
CHANNELS
0
200
400
600
800
1000
500
1000
1500
2000
40
80
120
160
200
250
750
1250
1750

Fig. 2

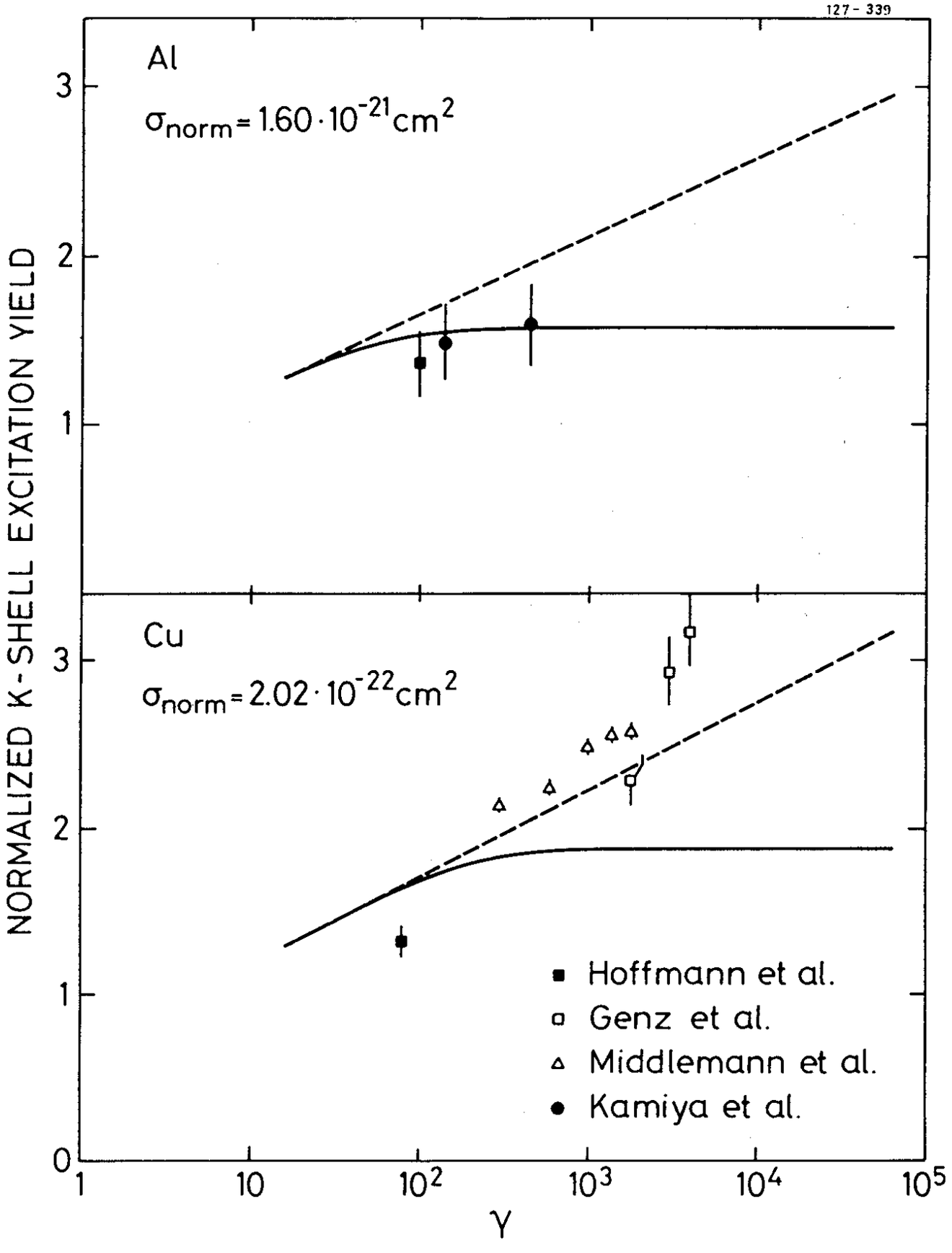
127 - 339
Al
$\sigma_{norm} = 1.60 \cdot 10^{-21} cm^2$
Cu
$\sigma_{norm} = 2.02 \cdot 10^{-22} cm^2$
NORMALIZED K-SHELL EXCITATION YIELD
γ
Hoffmann et al.
Genz et al.
Middlemann et al.
Kamiya et al.
0
1
2
3
1
10
10^2
10^3
10^4
10^5

Fig. 3

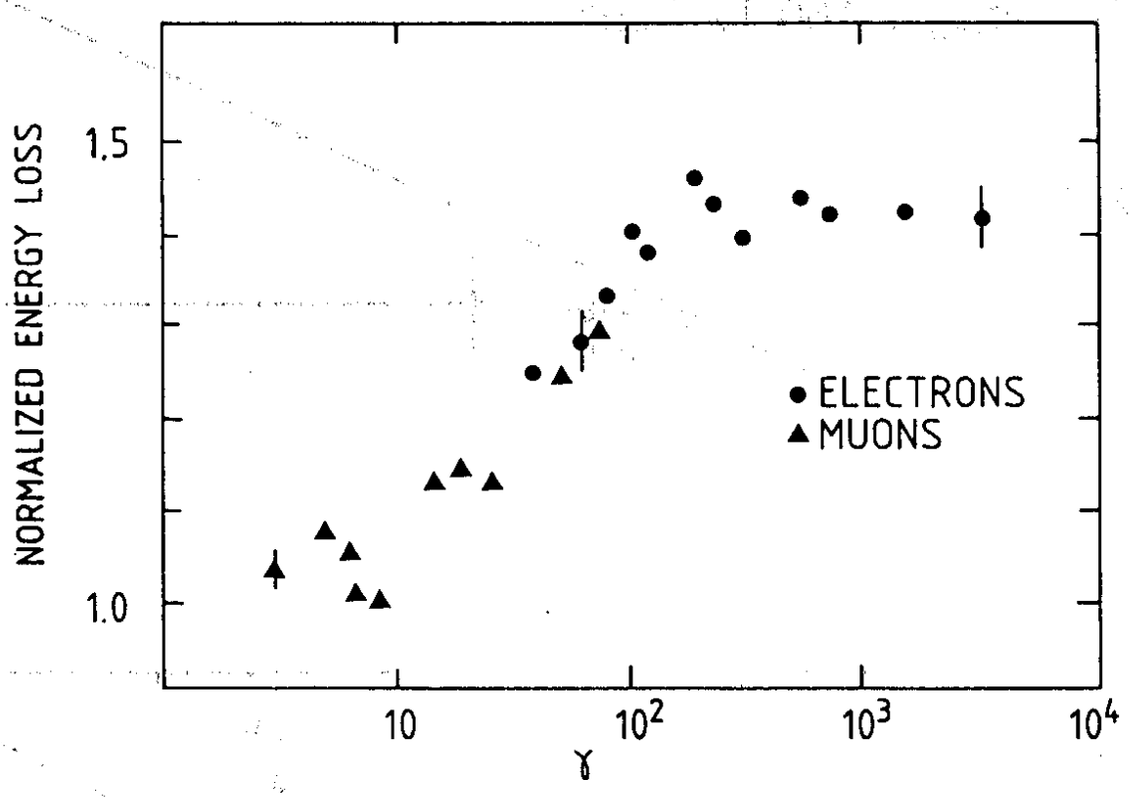
NORMALIZED ENERGY LOSS
1.5
1.0
10
10^2
10^3
10^4
γ
ELECTRONS
MUONS

Fig. 4

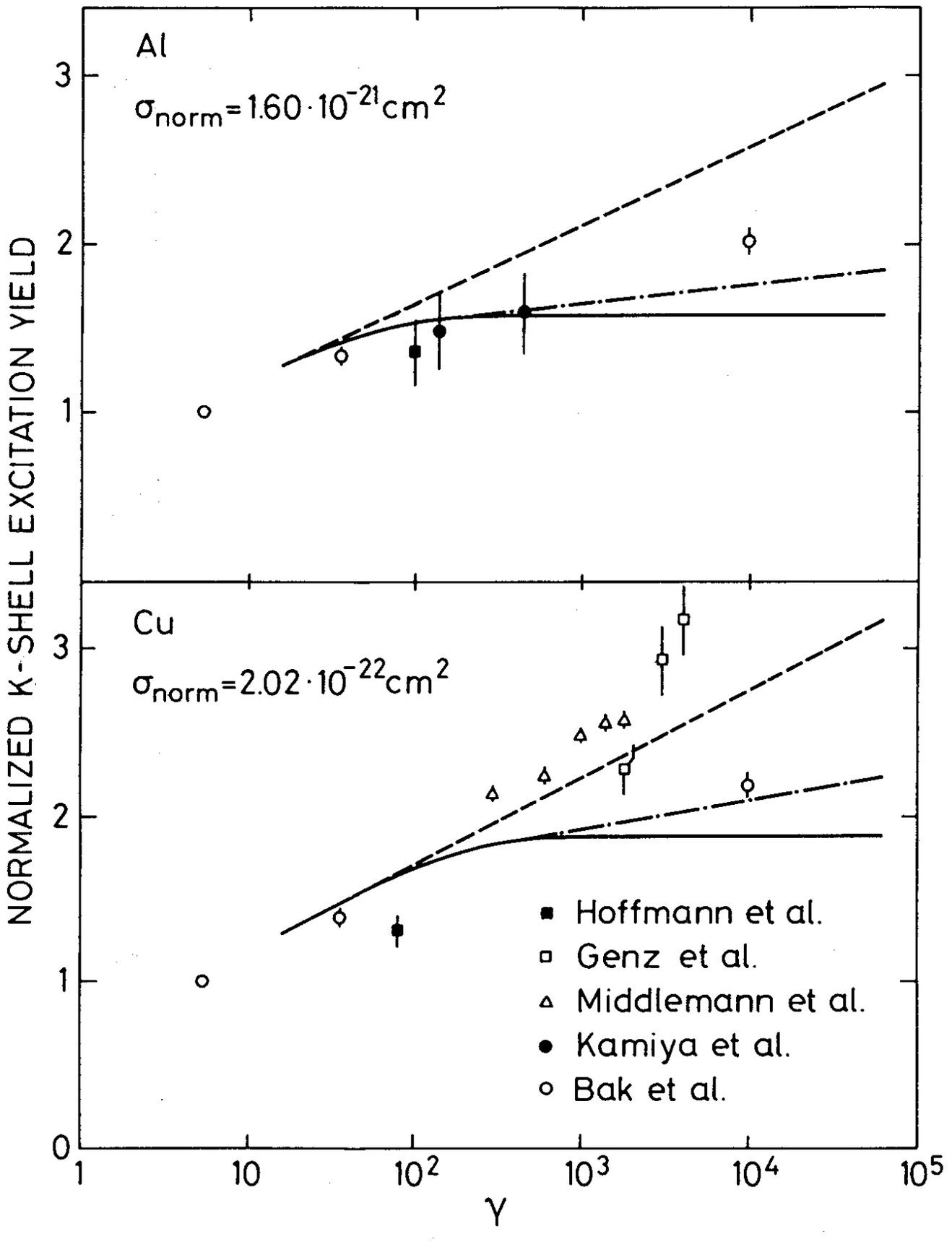
Al
$\sigma_{norm} = 1.60 \cdot 10^{-21} cm^2$
Cu
$\sigma_{norm} = 2.02 \cdot 10^{-22} cm^2$
NORMALIZED K-SHELL EXCITATION YIELD
γ
Hoffmann et al.
Genz et al.
Middlemann et al.
Kamiya et al.
Bak et al.

Fig. 5

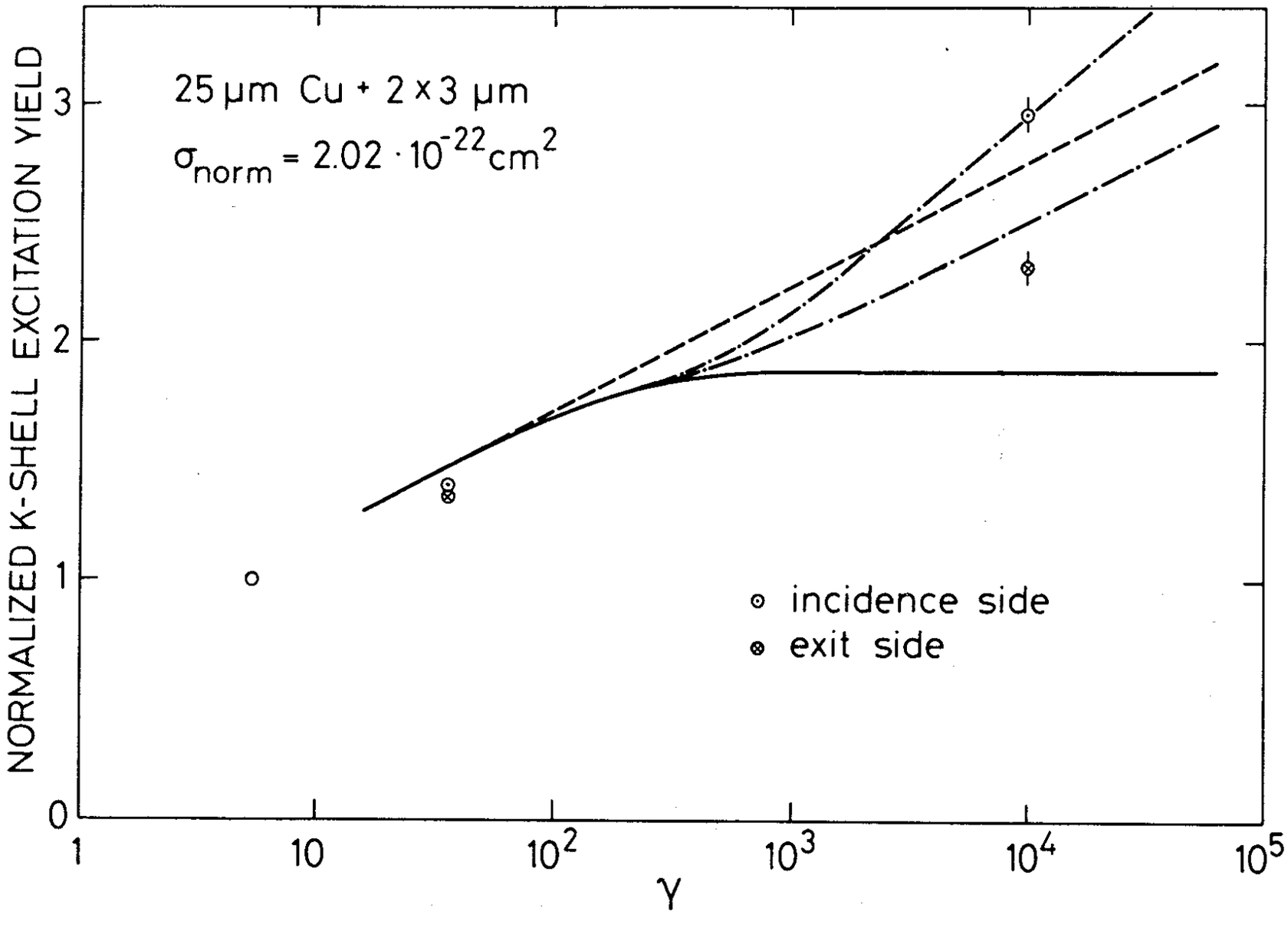
25 µm Cu + 2 x 3 µm
$\sigma_{norm} = 2.02 \cdot 10^{-22} cm^2$
NORMALIZED K-SHELL EXCITATION YIELD
0
1
2
3
1
10
10^2
10^3
10^4
10^5
γ
incidence side
exit side

Fig. 6